Environmental Earth Sciences (2024) 83:599
https://doi.org/10.1007/s12665-024-11896-5

ORIGINAL ARTICLE

2D nonlinear inversion of DC resistivity measurements, a case study; southeastern part of Ras El Dabaa, Northwestern coast, Egypt

Fardous Zarif[1] · Mostafa Barseem[1] · Ahmed Elshenawy[1] · Emin U Ulugergerli[2]

Received: 30 April 2024 / Accepted: 28 September 2024 / Published online: 17 October 2024

Abstract

The southern Mediterranean coast suffers from limited water resources as a result of exploitation of water supply, population growth, and climate change. Spatial lineaments and Seawater Intrusion (SWI) were detected at the southeast portion of Ras El Dabaa, on Egypt's northwest coast, using the direct current resistivity (DCR) method. The Vertical Electrical Sounding (VES) data were acquired using Schlumberger array along four profiles and inverted both independently and jointly, aiming to obtain Two Dimensional (2D) geoelectrical images. The results of the one Dimensional (1D) inversion of VES data at each profile were stitched to form pseudo-2D sections on which the resistivity values and aquifer thickness in the southwest of the region appeared to be generally increasing, indicating a potential improvement in water quality. However, the results did not fully image the lateral variation but focused on the horizontal boundaries of the subsurface. On the contrary, the results of 2D inversion of the same data sets successfully managed to provide images that depicted resistivity distribution in both lateral and vertical directions. The detected sets of lineaments and fractured zones within the oolitic limestone and fossiliferous limestone units control the occurrence of groundwater in the region. The 2D inversion scheme revealed a low resistivity zone that indicated the presence of SWI and/or the dissolution of marine salts from the marine limestone bedrock of these aquifers in the northern portions of the studied area. Additionally, analysis of the 2D apparent porosity section shows how aquifers are connected by secondary porosity, which is defined by structures that resemble channels. The current approach offers valuable structural information for future planning and development of such complex geological coastal locations, taking into consideration the vulnerability of the groundwater system.

Keywords Electrical resistivity · Vulnerability · Seawater intrusion · Groundwater · Egypt

Introduction

One of the most significant obstacles is the existence of carbonates for groundwater exploration in arid and complex geology coastal areas. Carbonate rocks dissolve readily in water. Cavities and other karst characteristics originate because the presence of fractures in carbonate rocks accelerates their deterioration. In these types of aquifers, the fracture networks are locations where groundwater mostly flows (Abu Risha and Sturchio 2018). Compared to the fracture network, the carbonate matrix has significantly low hydraulic conductivity (Cook 2003). As a result, the bulk of fractured carbonates consist of mixed level of porosity (Cook 2003). In the case of the coastal aquifers, saltwater intrusion accelerates the deterioration of the carbonate aquifer matrix and create complex subsurface structural pattern.

The Direct current resistivity (DCR) method is one of the vital tool for imagining the distribution of geo-electrical structures. This method involves injecting electrical current into the geological unit via two electrodes while simultaneously measuring the voltage difference between other two. The method has been extensively used in some subsurface investigations including environmental studies (Eze et al. 2022; César et al. 2017; Eleraki et al. 2010), mineral exploration (Kaidi et al. 2023), groundwater exploration (Alzahrani et al. 2022). Geoscientist deduce the existence and characteristics of a range of geological structures, including

✉ Fardous Zarif
fardous.drc@drc.gov.eg

1 Geophysical Exploration Department, Desert Research Center, Cairo, Egypt

2 Engineering Faculty, Department of Geophysical Engineering, Canakkale Onsekiz Mart University, Terzioğlu Campus, Çanakkale, Türkiye

bedrock, groundwater zones and geological boundaries, by analyzing the resistivity changes in the subsurface (Frischknecht et al. 1933; Flathe 1955; Henry-Poulter et al. 1933). The main goal is to obtain a full understanding of the subsurface resistivity distribution, lateral and vertical variations, and a more accurate representation of geological structures. These structural intricacies have a substantial impact on resistivity measurements, which might result in ambiguous subsurface interpretations. This study provides a potential method for enhancing the evaluation of DCR data via 2D inversion of VES data sets gathered individually.

Thereby providing a more profound insight into subsurface structure. Structural complexity is one of the major challenges to be solved. This issue requires spatially dense data set and appropriate software. Since the beginning of the 1970s, multi-dimensional inversion algorithms have been developed (e.g., Rijo et al. 1977; Loke and Barker 1996; Günther 2004; Marescot et al. 2005 Monte Santos et al. 2008; and Ulugergerli 2017) and used for 2D and 3D inversion of large data sets that are gathered with both conventional four-electrode and multi-electrode systems. Note that large scale studies targeting deeper parts of the subsurface still rely on the conventional VES applications (e.g., Uchida 1991; El-Qady et al. 1999; Özurlan et al. 2006; Khalil et al. 2011 and Massoud et al. 2015) in order to avoid cumbersome cable deployment.

Several geophysical approaches have been performed along the northern coast of Egypt to examine waterbearing aquifers and their properties. The evaluation of the DCR method and electromagnetic (TEM) method such as very low frequency (VLF) have revealed that the region has multiple geoelectrical layers, including alluvial deposits, limestone intercalated with clay, and saturated oolitic limestone (Zaghloul 2020; Hossam et al. 2021, 2023) and formation of waterbearing is highly fractured limestone (Zarif et al. 2018, 2021 and 2022). So far DCR method has only been applied to explore and identify the geometry of the groundwater aquifers (Zarif et al. 2018, 2021; Marina et al. 2021).

The southeastern part of Ras El Dabaa, northwestern coast of Egypt (Fig. 1) has been facing the challenge of geological complexity besides seawater intrusion (SWI) due to its proximity to the Mediterranean Sea (Saqr and Abd-Elmaboud 2024; Agoubi 2021; Eissa et al. 2016). Sets of structural lineaments striking in a NE–SW direction have an impact on the studied region (Abu Risha and Sturchio 2018). Groundwater recharge and occurrence are facilitated by these lineaments, which are represented by faults, fractures, and joints. The previous studies have assessed the risk of SWI in coastal areas and identified the features of the contact between brackish and seawater (Magesh et al. 2012; Atwia et al. 2013; Eissa et al. 2016, 2018). Previous studies have also proven that the DCR method provides valuable insights into the groundwater resources and aquifer characteristics of coastal areas; thus, in the frame of this research, the aim is to use 2D inversion of VES data to obtain more advanced information on the subsurface structure of coastal aquifer variability.

The 2D resistivity section, along with other geological and hydrogeological data, helps to determine the lineament structures and the extent and severity of SWI to allow appropriate management strategies to be implemented. By accurately identifying areas at risk of SWI, proactive measures can be taken to prevent further intrusion and ensure the long-term availability of freshwater for the local community (Elasy et al. 2018; Eissa et al. 2016). Additionally, this may provide valuable information for future planning and development in southeastern Ras El Dabaa, taking into consideration the vulnerability of the groundwater system. This study provided an important opportunity to advance the understanding of the 2D inversion of DCR data which is considered one of the vital methods to evaluate the groundwater potentiality and the coastal impacts of saltwater intrusion into shallow aquifers. The recent study on SWI in El Dabaa area investigated the effects of desalination brine injection and groundwater abstraction on the Middle Miocene aquifer in the El-Dabaa region. Their study predicted that the aquifer's potentiometric surface would drop to level of 1.4 m (Embaby et al. 2023). Adams et al. (2023) determined that the radius of the drawdown-affected area is roughly 550 m, with drawdown decreasing with distance from the extraction wells. The influx of reinjected water has an impact on the aquifer's salinity; by 2040, the maximum salinity at reinjection well sites will be 40,919 ppm, whereas at productive well sites it will be 37,860 ppm.

The hydrogeological context of this study area was prone to SWI problems; thus, a groundwater exploration survey was carried out there. The SWI problem require mapping the connections between the aquifers. DCR method and multi-dimensional inversion scheme provided images that depict of the subsurface resistivity distribution, in turn, geoelectrical models that represent geological setting. Questions have been raised regarding the extent to which the use of 2D joint inversion of VES data set enhances the accuracy and resolution of detecting subsurface geological, in comparison to traditional 1D inversion scheme.

Materials and methods

Investigated area

El Dabaa city is located in northern Egypt, and it is one of the cities of Matrouh Governorate. Its area is about 2,380 square km, and its population is about 30,000 people (Abu

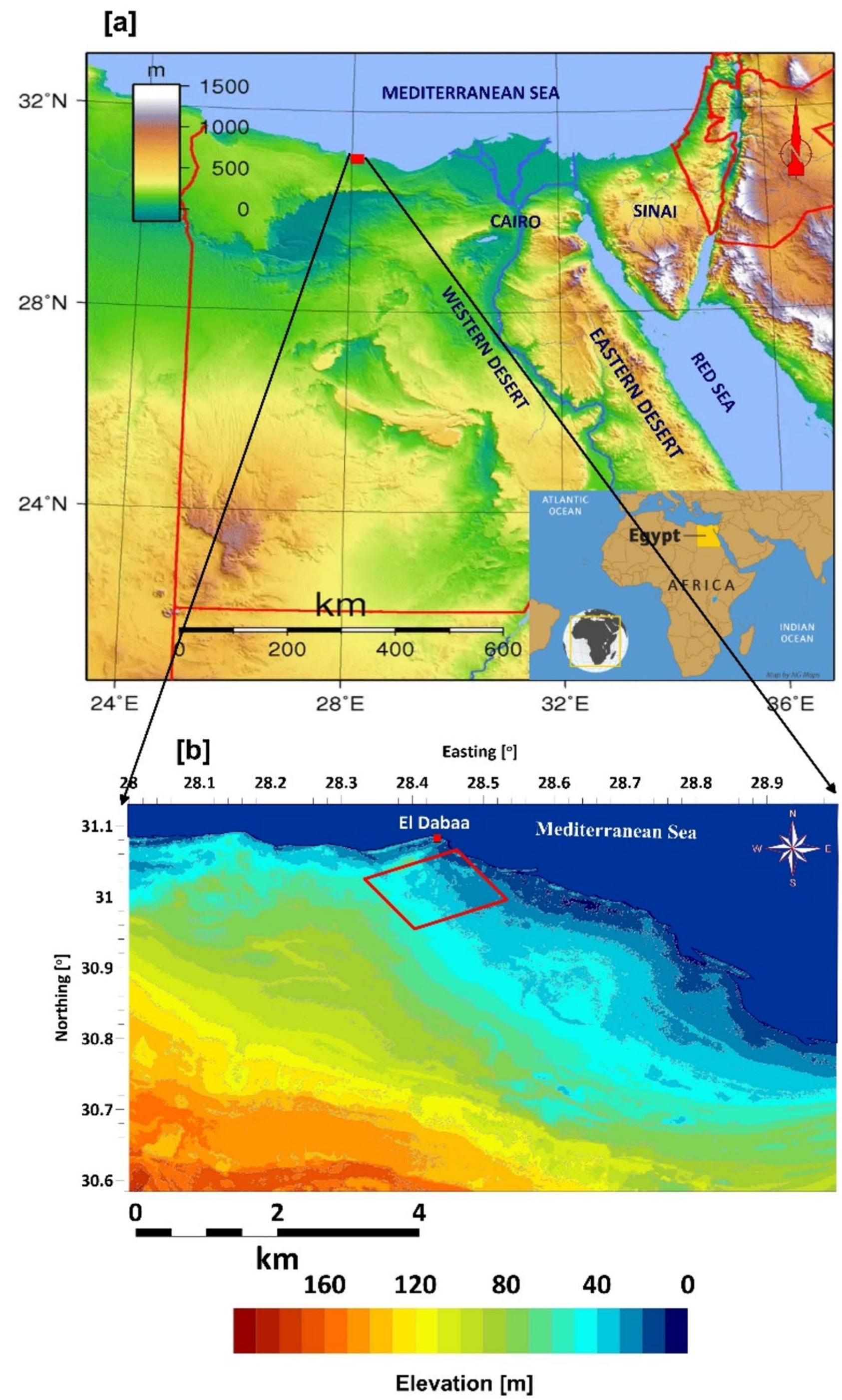

Fig. 1 [**a**] Topographic map of Egypt [**b**]Digital elevation map [DEM] for the investigated site. (source;-https://earthexplorer.usgs.gov), Red polygon pointed out to the study area

Risha and Sturchio. 2018). The city of El Dabaa is distinguished by its distinctive geographical location, as it is located on the coast of the Mediterranean Sea and is located near the city of Marsa Matrouh. This location made El Dabaa city an important tourist and commercial city. The city of El Dabaa has a recent history, as it was established in 2004 as a residential and commercial city as part of the project to establish the El Dabaa Nuclear Power Plant. The site is located in the northern part of the "Great Marmarican Homoclinal Plateau" in the southern Mediterranean Sea (Fig. 1). It has an arid environment, and the average ground surface elevation of the study area is around 40 masl. The investigated area is mainly surrounded by landforms that represent the integrated effects of several endo-genetic and exo-genetic characteristics, such as climatic conditions and lithological characteristics (Shata 1955, 1971; Abdallah 1966; Sayed 1967). The survey area is located southeast of El Dabaa (Fig. 1), where the Quaternary alluvial deposits and/or sand drift cover the limestone formation that serves as bed rock. Drainage lines, ridges, depressions, dunes, and southern tableland help govern surface runoff dispersion as well as groundwater recovery and storage. According to Abu Risha and Sturchio (2018), the area is organized into three fundamental geomorphologic sections running north to south (Fig. 2a). These topographical sections: a northern coastal plain with elevations ranging from 0 to 20 masl, a central piedmont plain situated between 20 and 50 masl, and a southwestern tableland reaching heights of 50 to 254 masl. An escarpment overlooking the coastal plain borders its northern side. The slopes of tableland borders are typically divided by the outlets of drainage systems that flow to the coastal plain from the sources located at high grounds. The current study area is situated in the piedmont plain, which is a transitional zone that stretches northward from the tableland and southward from the coastal plain.

The northwest Mediterranean coastal zone is composed of silt and sedimentary rocks, which span from the Tertiary to the Quaternary age, (Shata 1971). In the study area, the Miocene deposits are overlain by Pleistocene oolitic limestone, as illustrated in Fig. (2a). The subsequent deposits are of Quaternary origin. The Quaternary deposits consist of the Pleistocene Oolitic and cardium limestone, in addition to a slight coating of loamy deposits and drift sands that primarily cover low-lying areas and the floors of narrow valleys that intersect the tableland. This is followed by Miocene deposits, of the Moghra and Marmarica Formations (Fig. 2b). The base fluviatile to fluviomarine deposits are representative of the Moghra Formation. Its constituent parts include interbedded sand, shale, and argillaceous limestone. The limestone rocks that are higher in the composition of shallow marine origin, and their wide areal expansion is characteristic of the Marmarica Formation. It is the representation of the saline waterbearing formation and is composed of fragmented white limestone and a lower gray calcarenite with some shale intercalation. There are some minor structural undulations in the form of broad monocline structures or mild upfold and downfold structures (Yousif and Bubenzer 2015). The majority of folded structures have a NE-SW orientation in Fig. (2a). Several significant faults in the area have downslopes that face north (Abu Risha and Sturchio 2018). According to Abu Risha and Sturchio (2018), the water supplies in the studied area are recharged by the available precipitation. Some of landforms affect groundwater storage and accumulation are the local part of tableland, ridges, topographic depressions, length of the dunes, and drainage networks. These features also control the dispersion of surface runoff.

Pleistocene oolitic limestone and middle Miocene aquifers are the two categories into which the aquifers in the area under study and its environs may be divided. The Pleistocene limestone stretches about 10 km southward. It is considered the most important aquifer along the coastline. The coastal oolitic limestone ridges have fewer cementing elements than the inland ridges. The ridge sides are covered with loose shoreline sand accumulations that allow rainfall to infiltrate and percolate directly. Groundwater exists as a free water table (phreatic state). It rises to near-mean sea level, which is caused by local percolation on the coastal

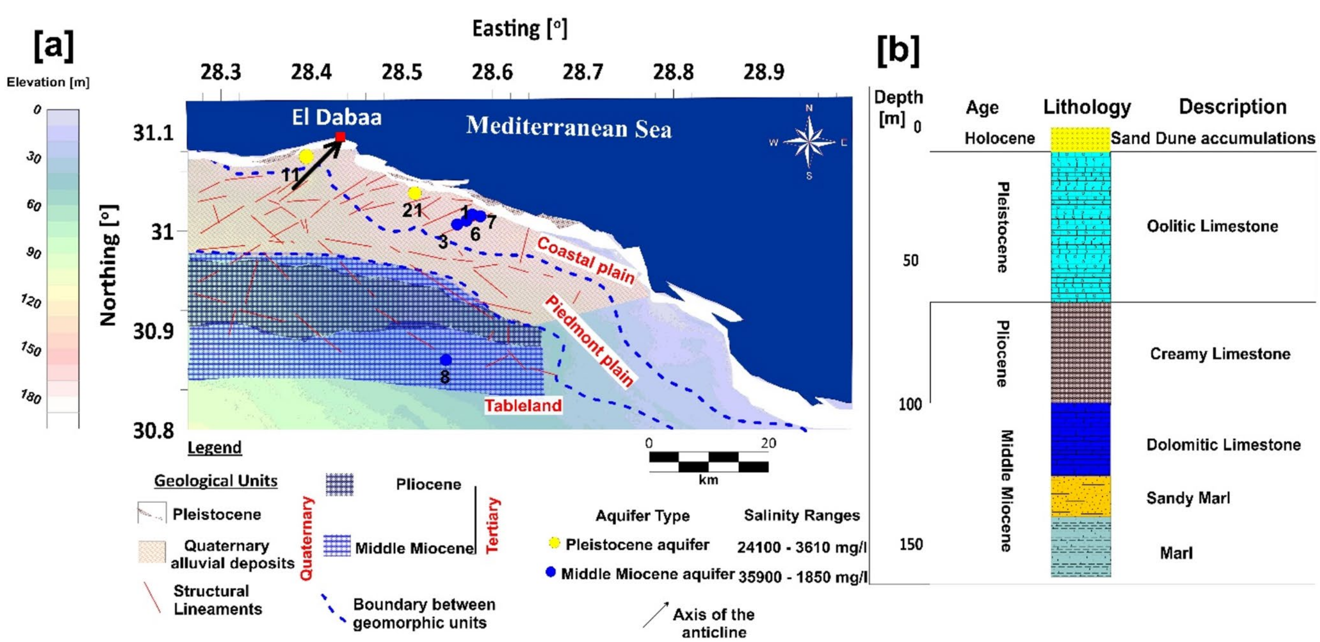

Fig. 2 [**a**] Geomorphological and geological units of the study area, [**b**] Idealized stratigraphic section at El Dabaa area, (after Abu Risha and Sturchio 2018)

plain and the intrusion of seawater. The horizontal flow from the Mediterranean creates a saline water table that is topped with a thin layer of fresh water. This phenomenon is a result of the natural equilibrium between both the excess of recharge from precipitation and the outflow through seepage toward sea (Abu Risha and Sturchio 2018).

The Marmarica aquifer, which is made of shale, dolomite, and limestone, is a representation of the aquifer of the Middle Miocene age. It is mostly fractured and may be found in a series of horizons with sporadic sandstone bands in between impermeable clays. The productivity of the aquifer is impacted by lateral and vertical facies variations, especially in the coastal region. The Marmarica aquifer's groundwater naturally empties into the Mediterranean by subsurface flow. It comes from local rainfall and takes the shape of thin sheets that build up when they come into touch with impermeable clay (semi-confined water). According to Yousif and Bubenzer (2015), this aquifer is divided into two distinct waterbearing units: the lower unit is composed of marly limestone, and the upper one is composed of white chalky limestone. There are many hydro-geophysical studies on the study area and its vicinities focus on different features of the aquifers. (Sayed 1967; Abdel Latif 1973; Maghraby 1997; Fouad 2001; DRC 2005 and 2008; Housny 2011; Abu Risha and Sturchio 2018; Kotb et al. 2018). Kotb et al. (2018) applied the DCR method and 1D inversion of VES data sets. Their layered earth model demonstrated that the upper part of the oolitic limestone act as the shallow aquifer in this region. This aquifer is subdivided into two zone; the bottom zone is saline as a result of saltwater intrusion, whereas the upper zone is brackish (Kotb et al. 2018). Our study used the same data set of Kotb et al. (2018) however, we employed somewhat different approaches and allowed our interpretation scheme to delineate both horizontal and vertical variations via 2D inversion rather than retaining imaginary layered units.

DCR method

We used Schlumberger array to collect the vertical electrical sounding (VES) data. The Schlumberger array is frequently employed in electrical resistivity surveys due to its numerous benefits. These include its high sensitivity to vertical resistivity changes, straightforward data interpretation, and capacity to achieve deeper ground penetration with minimal distortion. By adjusting electrode spacing, this configuration enables a wide range of investigation depths, making it adaptable to various geological settings. Furthermore, it excels at identifying subsurface features such as aquifers, mineral deposits, and contamination zones. After injecting electrical current from two current electrodes (A and B), the potential difference between the other two potential electrodes (M and N) is measured. We derived apparent resistivity (ρ_a) using current (I), potential drop (ΔV), and geometric factor (K) via Ohm's law. Equation (1):

$$\rho_a = K\Delta V/I \tag{1}$$

Since each ρ_a data take into account, the effects of both the array of electrodes and the contribution of geo-electrical structures around and underneath the electrodes, the apparent resistivities are not appropriate to image the subsurface directly (e.g., Merrick 1997). As a common practice, the VES data were gathered individually and inverted with 1D inversion scheme that produce layered models (e.g. Vedanti et al. 2005; Ekinci and Demirci 2008). However, a 2D model is required due to the difficulties of imaging the subsurface. Thus, a pseudo 2D image was generated using layered earth models for further examination. Thus, we employed 2D inversion scheme to obtain 2D resistivity section for further evaluation.

2D nonlinear iterative inversion scheme

To image the lateral discontinuities of the aquifer units a 2D earth model (Rijo et al. 1977; Uchida 1991) is required. To conduct a 2D inversion of individual VES data we should meet two criteria. First, all VES stations must be obtained along the same profile and, in line with each other (Fig. 3a). The expansion of current electrodes (A and B) can't deviate from the profile by no more than a few degree (Fig. 3b). Second, the overlapping between the adjacent VES stations should be less than the maximum AB expansions (e.g., Ulugergerli 2017; Ertekin and Ulugergerli 2022).

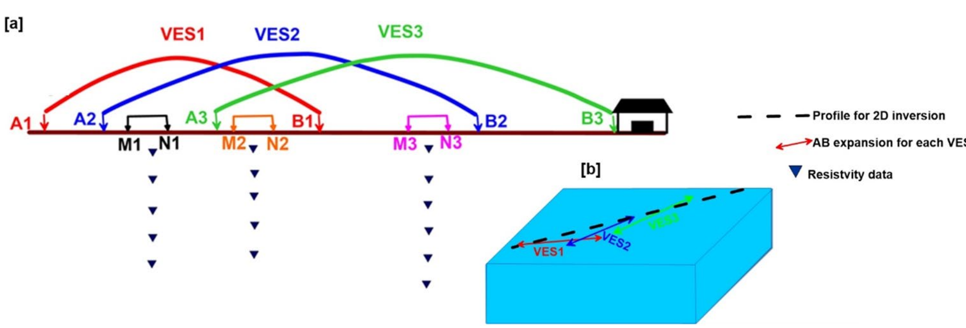

Fig. 3 [**a**] Distribution of VES points along a profile, [**b**] the AB expansion for each VES

2D image of the geoelectrical structures underneath the profile may then be obtained using a 2D inversion scheme. The following is an equation for the ill-posed and nonlinear inversion problem regardless of the dimension of the model (Menke 1989; Meju 1994):

$$\Delta p = (J^T J + \beta I)^{-1} J^T \Delta D \tag{2}$$

Where: Δp is the logarithmic update vector for the initial model parameters (p) which is the logarithm of conductivity. The vector ΔD represents the difference between logarithm of measured (ρ_a^o) and computed (ρ_a^C) apparent resistivity, respectively. J is a matrix composed of partial derivatives and β is the smoothing coefficient I is the identity matrix. (for more details, see Ulugergerli 2017). The measure of misfit, e, is given as:

$$e = (\Delta D^T \Delta D/N)^{(1/2)} \tag{3}$$

Where T is transpose while N is number of data. The inversion code iterates until either the misfit reaches an arbitrarily selected threshold value or the number of iteration reaches to user defined value.

Survey

Kotb et al. (2018) acquired 27 VES stations along four profiles (Fig. 4a). The range of AB/2 varies between 1 and 2000 m while MN\2 varies from 0.5 to 250 m. Wherever MN increases, two successive AB/2 have double reading for both MN intervals to overcome low potential difference. All segments of the apparent resistivity curves were shifted to match to first (MN\2 = 0.5) segment (Ertekin and Ulugergerli 2022). This procedure is equivalent to gather VES data using only first MN/2 value.

Results and discussion

1D inversion

Kotb et al. (2018) used the commercial program IX1D (version 3, Interpex 2023) in order to determine the resistivity and thickness of the geoelectrical units (Figs. 5, 6, 7 and 8b). The 1D inversion process involves two-stage process; (a) using a layer for every data point to build smooth models. Constable et al. (1987) termed this technique Occam's inversion as it uses thicknesses created automatically from the AB spacing data, which remain constant throughout the inversion, the resistivities of imaginary layers are updated by the inversion and (b) from the result of the Occam inversion, a small number of layers (i.e., 5 or 6) were chosen, and their resistivity and thickness were simultaneously estimated by 1D inversion. The obtained pseudo-sections (Figs. 5, 6, 7 and 8b) are all stitched and correspond to the same profiles (Fig. 4a). According to Kotb et al. (2018), the bottom layers are distributed rather evenly over the entire area. Low resistivity measurements, which are indicative of clay content or seawater-saturated soil, are also present in the majority of the studied area.

It is apparent that the area's relative resistivity values are higher on the western side where the dense limestone

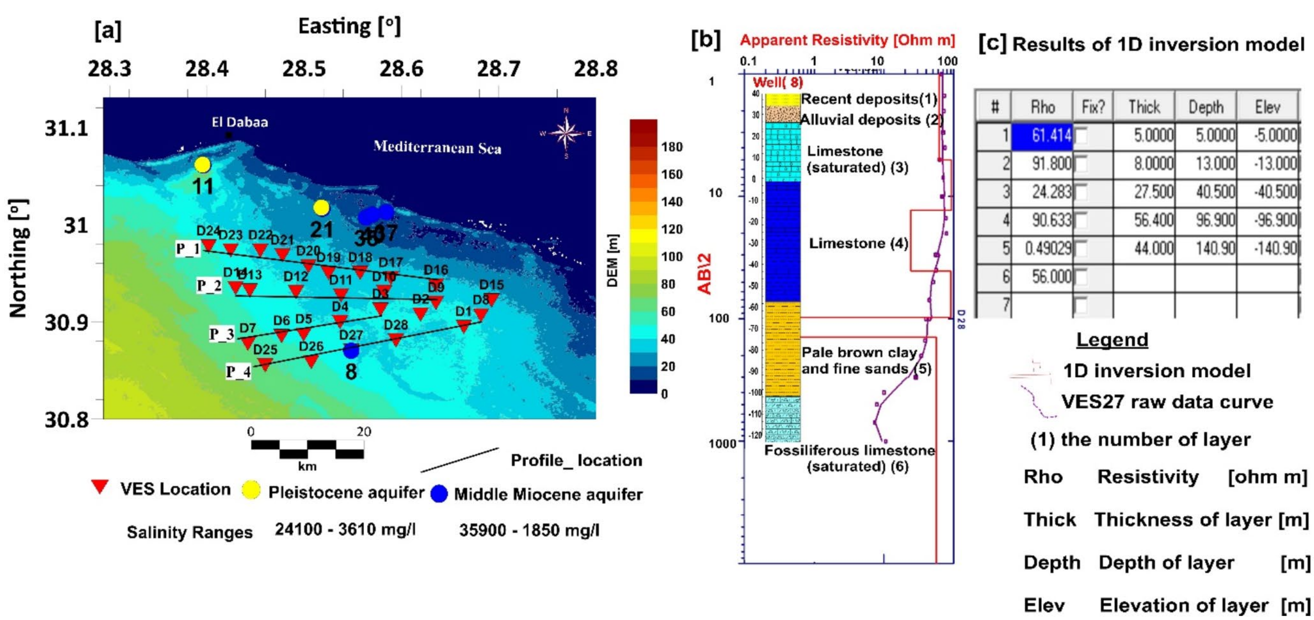

#	Rho	Fix?	Thick	Depth	Elev
1	61.414		5.0000	5.0000	-5.0000
2	91.800		8.0000	13.000	-13.000
3	24.283		27.500	40.500	-40.500
4	90.633		56.400	96.900	-96.900
5	0.49029		44.000	140.90	-140.90
6	56.000				
7					

Fig. 4 [**a**] Distribution of VES points over the investigated area and location of electrical resistivity profiles, [**b**] Example for 1D VES interpretation (D27) and lithology of Well no.8 and [**c**] represents the results of 1D inversion of VES27

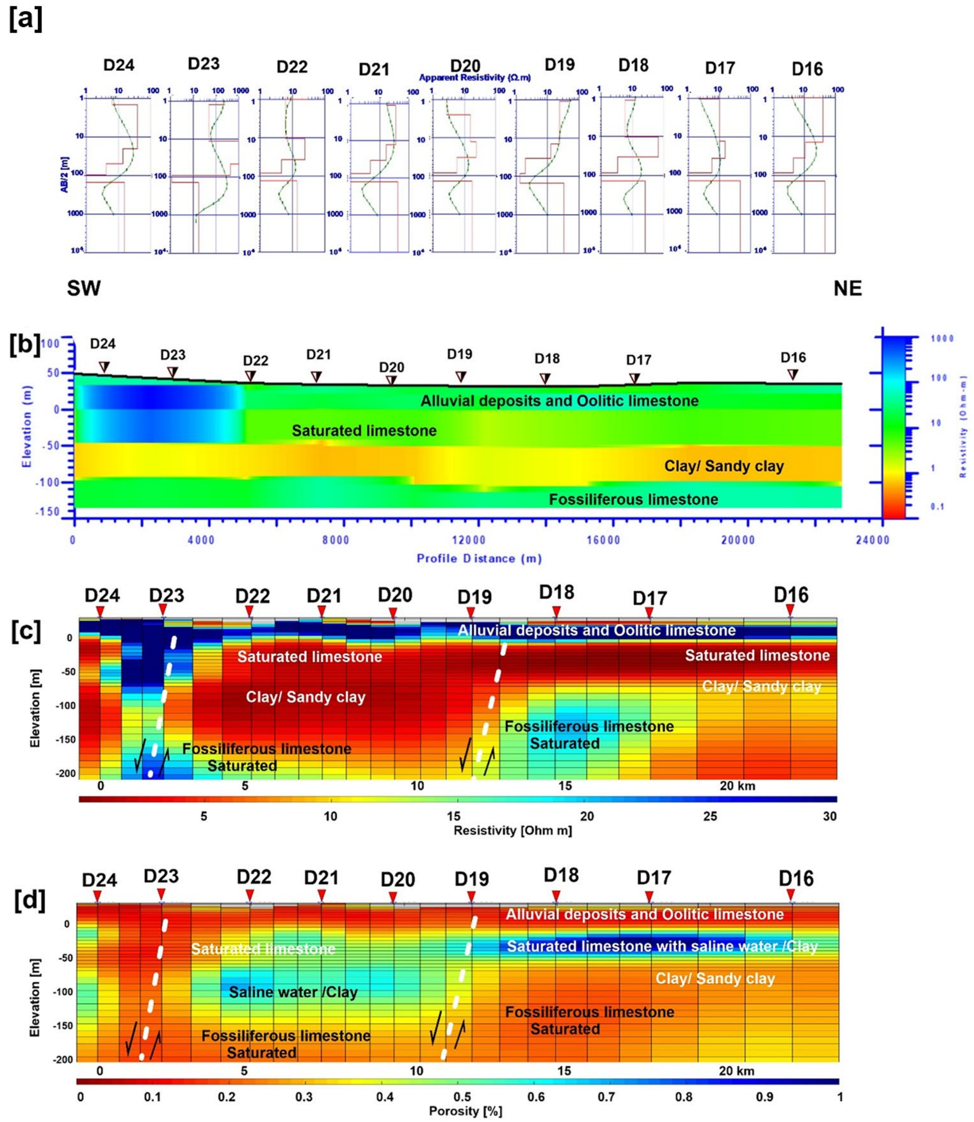

Fig. 5 [**a**] Observed VES curves (green marks), calculated curves (green line) and inverted 1D model (red line) [**b**] inverted1D cross-section #1, [c] 2D inversion models of resistivity and [d] pseudo 2D porosity section of profile-1(#p1), dashed white line represents inferred lineament structure form 2D inversion

is found (Layers 1,2 and 6) than they are in the other directions where fractured limestone is expanded. Figures (5–8 b) depict the primary six geoelectrical layers, which are the average values of resistivities and thicknesses derived from the calculation of each individual curve. These average values of resistivity and thickness from the top to bottom are as follows: 50.5 Ω.m and 1.8 m, 76.5 Ω.m and 14.7 m, 74.7 Ω.m and 20.9 m, 69.1 Ω.m and 50.9 m, 1.1 Ω.m and 50.6 m, and 35.75 Ω.m, respectively. The resistivity values of all layers are generally consistent, except for the fifth layer, (Figs. 5, 6, 7 and 8b). where variations occur due to differences in clay and limestone concentration along geoelectrical cross sections. Recent deposits (loose sand and rock debris) correlate to the topsoil surface layer; alluvial deposits are represented as the second layer; and detrital oolitic limestone underlies all. This assessment was carried out utilizing the accessible lithological description from the nearest well, such as well no. 8, to the VES no D27 (Fig. 4b).

2D inversion

2D resistivity sections were obtained using an inversion algorithm after Ulugergerli (2017). For improved visibility, the color scales were constrained between 0.3and 30 Ω.m (Figs. 5c, 6, 7 and 8c). Figures 5c and 8c show the comparison of the results of both 2D and 1D inversions. The Archie's empirical equation was added to the current experiment (Archie 1942). Archie's law (Archie 1942) states that the volume and resistivity of water in a soil pore have an empirical relationship with the resistivity of the formation as shown in Eq. (4).

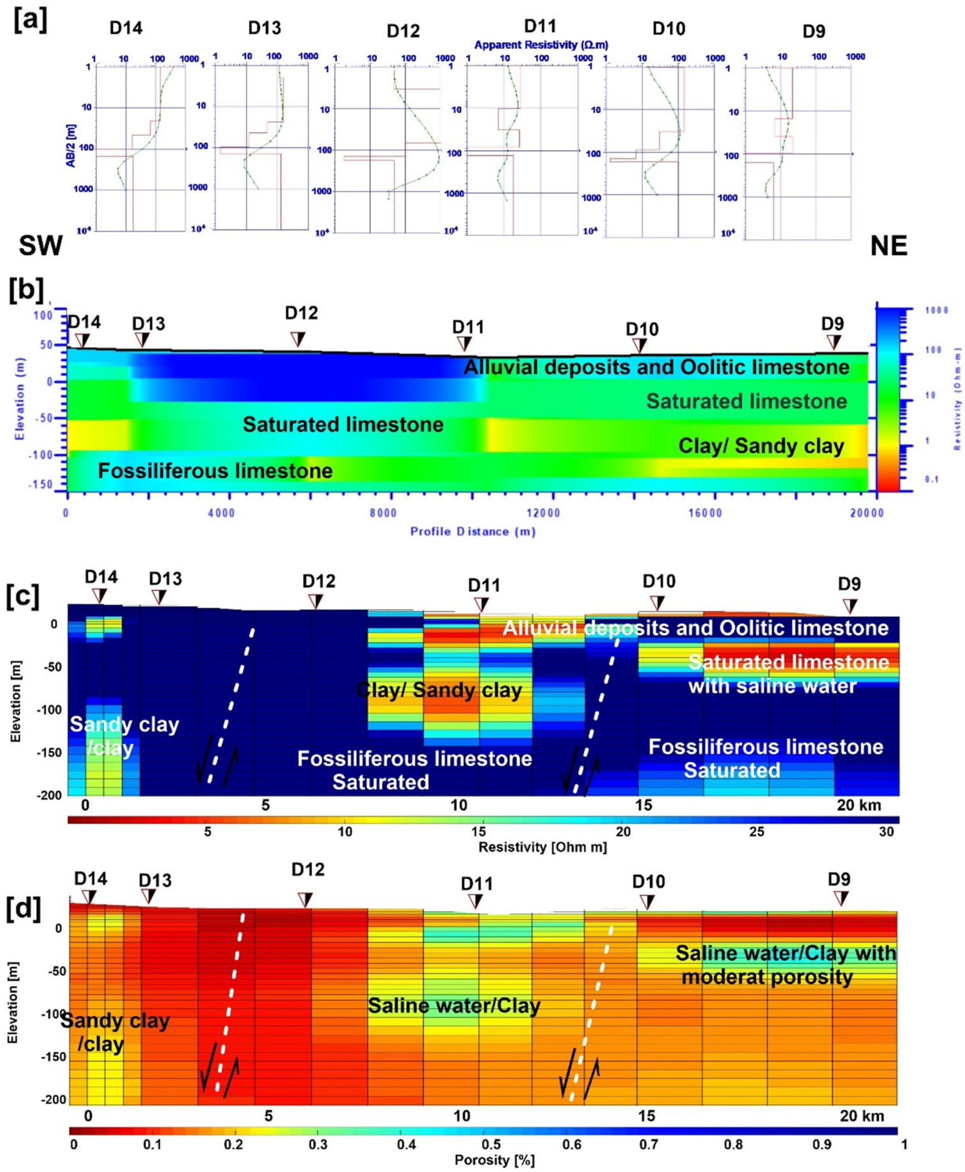

Fig. 6 [**a**] Observed VES curves (green marks), calculated curves (green line) and inverted 1D model (red line) [**b**] inverted1D cross-section #2, [**c**] 2D inversion models of resistivity and [d] pseudo 2D porosity section of profile-2(#p2), dashed white line represents inferred lineament structure form 2D inversion

$$\frac{\rho}{\rho_w} = a\phi^{-m} S_w^{-n} \tag{4}$$

where S_w is the proportion of water-filled pores in the volume (water saturation), ∅ porosity, ρ bulk resistivity, ρ_w water resistivity, and n and m are empirical constants related to the rock type. It should be noted that Archie's law only holds true if the geological unit has no clay and a non-conducting matrix (Glover et al. 2000). The sandy clay unit in region may lead to rather unrealistic results due to lacking of enough resistivity contrast (Glover et al. 2000). Taking into consideration this assumption a 2D porosity section is produced, employing a possible scenarios of seawater intrusion. In this study we used ρ_w = 0.3 Ω.m, which is significantly lower than the resistivity of the nearby clay unit (Figs. 5, 6, 7 and 8c). The interpretation of porosity in this model is influenced by choosing a low resistivity value for seawater (0.3 Ω.m). seawater has a known average electrical resistivity due to its dissolved salts, primarily sodium chloride (NaCl). The resistivity of seawater is generally around 0.2 to 0.5 Ω.m, with 0.33 Ω.m often used as a representative value. This value accounts for the saline concentration typical of coastal environments. Areas affected by seawater intrusion will exhibit reduced resistivity measurements. By incorporating an appropriate seawater resistivity value, the model can effectively capture the range and influence of seawater intrusion on the distribution of porosity (Luz and Régis 2009; Goto et al. 2008). For the pseudo 2D porosity section, the resistivity values obtained from 2D inversion used as bulk resistivity values for each cell (Figs. 5, 6, 7 and 8d) (Fajana 2020). We assume S_w =1 and the constants a, m and n are 1, 2.5 and 2 respectively. Porosity is derived from

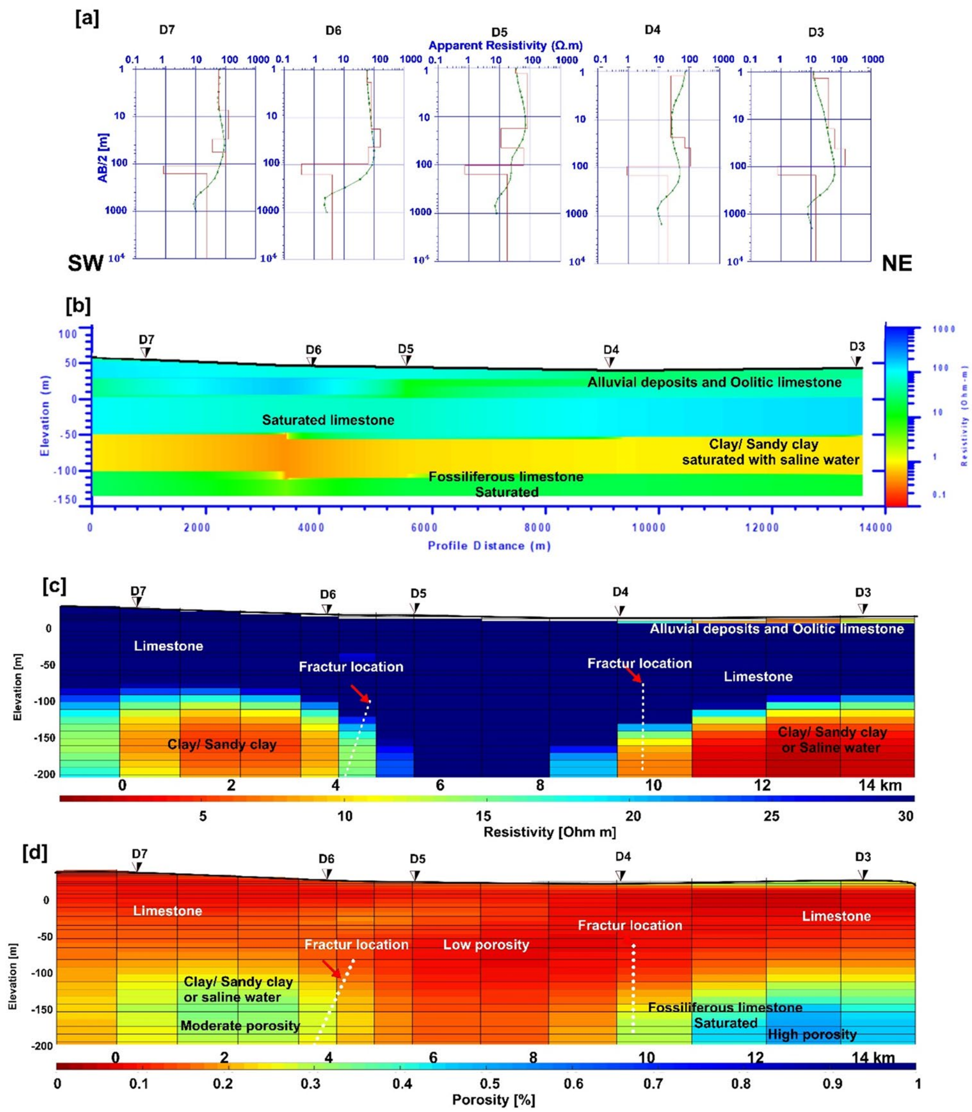

Fig. 7 [**a**] Observed VES curves (green marks), calculated curves (green line) and inverted 1D model (red line) [**b**] inverted1D cross-section #3, [**c**] 2D inversion models of resistivity and [**d**] pseudo 2D porosity section of profile-3(#p3), dashed white line represents inferred lineament structure form 2D inversion

resistivity data using empirical relationships that involve m and n. The porosity calculation follows:

$$\phi = \left(\frac{a(R_a/R_w)}{S_w^n}\right)^{\frac{1}{m}} \quad (5)$$

Where:

R_a is apparent resistivity and R_w is water resistivity.

Nine VES stations were obtained along the 23-kilometer of profile-1 (P#1) which is shown in Fig. (4a). Table (1) shows that the model smoothing coefficient was set 0.5, which is the result of trial and error test. The misfit dropped from 41 to 3.8 after 65 iterations of the code. A final fractal variation of fit, 0.00073991(dmisfit) is achieved. The final estimated model's resistivity value ranged from > 30 Ω.m to 0.1 Ω.m. Figure (5c and d) show the final results, whereas the layered model shows a reasonably consistent subsurface. 2D inversion reveals possible fault zones and barriers between VES stations D19 and D20 and between D22 and D23.The resistivity contrast is between D18 and D19, which is the possible fault zone. 2D apparent porosity-section reveals that SWI at the most of VES stations at depth from 0 m to 50 m in the NE direction and from 50 m to 100 m in the SW direction with low resistivity around 1 Ω.m, where the possibility of saturated limestone is located. The results show that the apparent porosities vary between 0.6 and 0.8 for low resistivity zones (Fig. 5d).

Second profile (P#2) is 22 km long and consists of 6 VES stations (Fig. 4a). The model smoothing coefficient and analysis parameters are listed in Table (1). Figure (6c) display the resulting model, the resistivity values were found to be 0.9 and more than 30 Ω.m. 1D model does not reveal any lineament structure while 2D inversion point out that water bearing limestone is highly fractured. The evidence for SWI is also appeared along (P#2) below VES stations

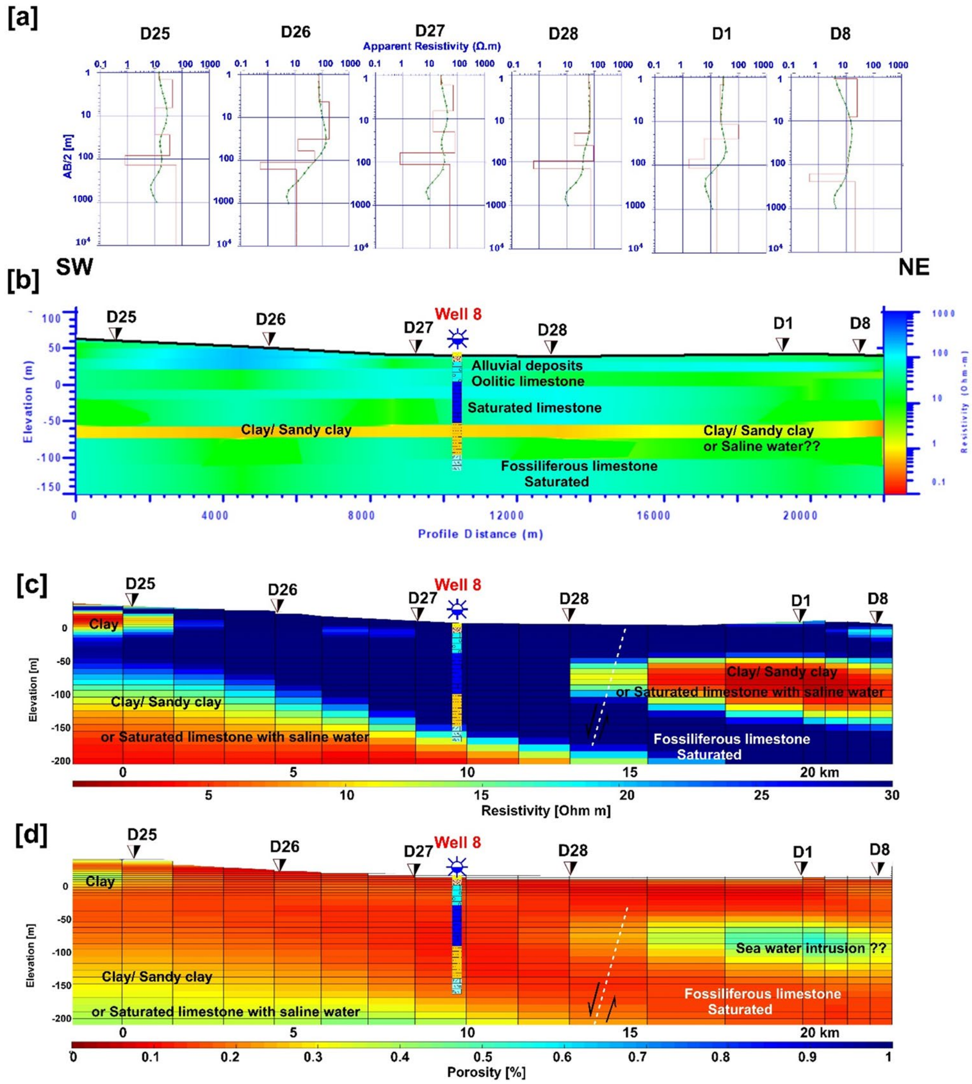

Fig. 8 [**a**] Observed VES curves (green marks), calculated curves (green line) and inverted 1D model (red line) [**b**] inverted1D cross-section #4, [**c**] 2D inversion models of resistivity and [**d**] pseudo 2D porosity section of profile-4(#p4), dashed white line represents inferred lineament structure form 2D inversion

Table 1 Variation of misfit values in 2D inversion

Profile No.	Length (km)	No. of VES stations	Smoothing coefficient	No. of iteration	Initial and last Misfit values	Final fractal variation of fit (dmisfit)
P1	23	9	0.5	65	40.6–3.8	0.0007399
P2	22	6	0.5	87	16.5–0.7	0.000978
P3	15	5	0.5	80	33.7–2.7	0.0006445
P4	22	6	0.5	87	16.5–0.7	0.00097795

D9 and D10 from depth 0 to 50 m with low resistivity less than 1Ω.m in the direction of NE where Mediterranean Sea. Two faults are detected between VES stations D10 and D11 and between D12 and D13. What is interesting in this results that 2D apparent porosity section is around 0.6–0.7 under the same location of low resistivity zone which confirm and support the possibility of SWI.

Profile (P#3) is given in Fig. (7) and shows a 15-kilometer-long profile with five VES stations (Table 1). The predicted resistivity values along (P#3) were found to range between 0.8 and > 30 Ω.m in the last model. Once more, the 1D model displays rather homogenous layered earth; however, between VES stations D4 and D5, a significant fault/fracture zone was discovered by the 2D inversion. This zone is also visible in 2D apparent porosity section. At depths of 100–150 m, apparent porosity is around 0.6–0.7 beneath VES stations D3 and D4 in the NE direction, as well as under VES stations D5 and D6 in the SW direction. These areas could exhibit clay or saline water-saturated fractured limestone (Fig. 7d).

Forth Profile (P#4) is the final one, measuring 22 km in length (Table 1). Together, the DCR data from six stations were inverted (Fig. 8a-d). The misfit reduced from 16.5 to 0.7 after 87 iterations of the algorithm. Between consecutive iterations, the ultimate fractal variation of misfits was 0.00097795. According to the structural geology (Fig. 2c), a normal fault is inferred between VES D28 and D1 in Fig. (8). From surface to bottom, the geological succession (well 8) that has been documented is as follows: oolitic limestone and alluvial deposits can't be distinguished from one another because of their comparable resistivity range (> 20 Ω.m). The layer's bottom ranges in depth from 77 m below VES D1 to 200 m at VES D25. This layer locates on top of a sandy clay layer with low resistivity (< 7 Ω.m). At a depth of 50 m, there is an intriguing feature (SWI) that extends from VES D1 to VES D8. Due to previous studies, certain aquifers are dominated by brackish water (Eissa et al. 2018; Yousif and Bubenzer 2015). The outcomes of the 2D apparent porosity assessment reveal that high values (0.6–0.7) correspond to fractured limestone containing brackish water, which is consistent with the 2D resistivity data. The most significant result from the data is that the 2D inversion findings indicate that local faults disrupt and seal the aquifers. As a result, certain aquifers are shielded, and the threat of SWI is averted. Both safe and potentially polluted sections can be identified in the water-bearing parts of the oolitic limestone. Consequently, the predicted structural lineaments align with the results of Yousif and Bubenzer (2015), indicating that sets of faults striking in the NE-SW direction had an impact on the area (Fig. 10). These lineaments are represented by joints and cracks that allow groundwater to flow and be recharged.

The structures depicted in Figs. 5c, 6, 7 and 8c align with the geological characteristics of the region, as shown in Fig. 2c. The sequence, arranged from surface to bottom, consists of alluvial deposits and oolitic limestone that have similar resistivity ranges (> 20 Ω.m), making them indistinguishable. Along the profile, the layers' depths vary between 40 and 50 m (P1) and are located on a low-resistivity (< 7 Ω.m) saturated layer of limestone or clay. As illustrated in Fig. 6, these features form a barrier and extend to a depth of 200 m. In limestone, conductive zones (< 10 Ω.m) may arise from secondary porosity, which are fractures filled with seawater or clay, as shown in Figs. 5d, 6, 7 and 8d. The distribution of subsurface resistivity and apparent porosity across the study area is shown in Fig. 9 at various depths from the surface to 100 m (Fig. 9a, b, c, d, e, and f). Fence diagrams (Fig. 9g) represent the potential three-dimensional distribution of resistivity throughout the study area at a depth of 150 m, where Fig. (9 h and i) show the pseudo-3D fence diagrams of apparent porosity and highlight the locations of secondary porosity that impact the connection between aquifers as a channel-like structure between VES D24 and D23, as well as between VES D22 and D2. This results, given the explanation provided, it is evident that the presence of fractured zones within the oolitic limestone and fossiliferous limestone layers influences the occurrence of groundwater. It is somewhat surprising that the porosity calculation was ambiguous in this condition. The resistivity of the layers varies from one location to another, according

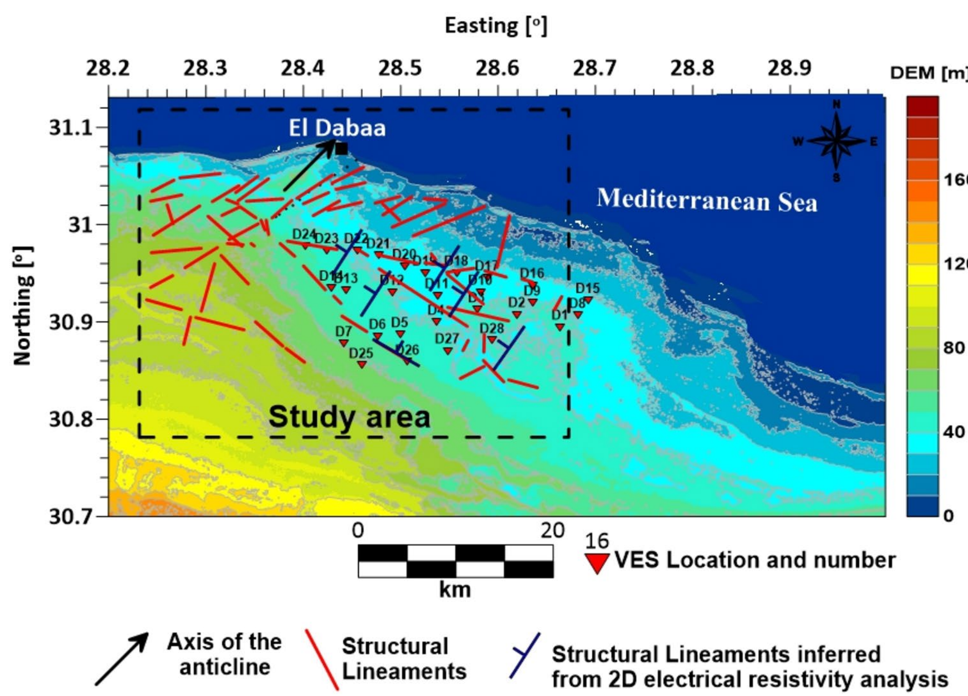

Fig. 10 Digital elevation map with structural lineaments inferred from 2D electrical resistivity analysis beside the geological structural lineaments after (Abu Risha and Sturchio 2018)

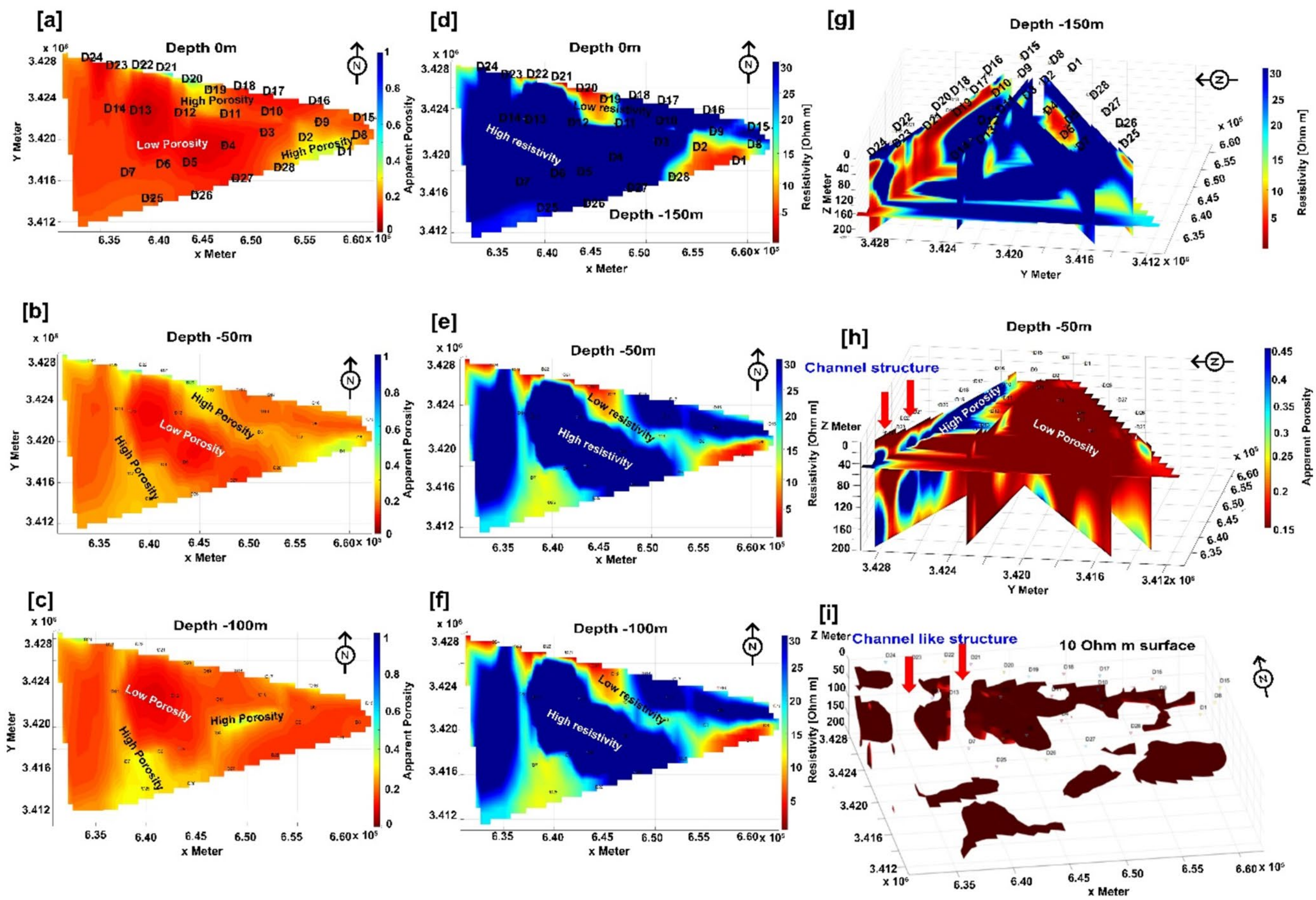

Fig. 9 The distribution of subsurface resistivity and apparent porosity [**a**] porosity section from the surface, [**b**] porosity section at depth 50 m, and [**c**] porosity section from at depth 100 m. [**d**], [**e**] and [**f**] the distribution of resistivity at depths 0, 50 and 100 m.[**g**] 3D fence diagram for 4 2Dprofiles at depth 150 m, [**h**] 3D fence diagram for apparent porosity at depth 50 m. and [**i**] 3D fence diagram for apparent porosity at resistivity 10 Ω.m, red arrows pointed out to the location of the predicted channel-like structure at the northwestern part of the study area

to the interpretation of the VES data across the entire studied area (Kotb et al. 2018). The medium resistivity readings of the third geoelectrical layer, which range from 10 to 25 Ω.m, suggest the presence of groundwater at all VES soundings. The low resistivity measurements may be attributed to an increase in water salinity or clay content.

Based on the hydrogeological data currently available for the region under investigation, both surface runoff and local precipitation penetrate the ground to replenish the water-bearing layer. The central portion of the region was deemed the optimal location for drilling production wells as the resistivity values and aquifer thickness increased towards the southwest. This is due to the increased potential for water quality and better well production in that direction. In the northern region of the study area, a low resistivity zone identified by the 2D inversion scheme indicated the presence of saltwater intrusion (SWI). These results align with those of Embaby et al. (2023). The waterbearing layer was discovered at varying depths, with the greatest depth found in the south and decreasing towards the north. This finding is consistent with the research of Adams et al. (2023). The freshwater-bearing layer ranged in thickness from 15 to 25 m, and SWI appeared at a depth of approximately 10 m in the northeast, as reported by Eissa et al. (2018). At a depth of around 120 m, every layer was inundated with saltwater, according to Sampson et al. (2018). This survey provides valuable insights into the extent and effects of SWI in the coastal area, particularly in the vicinity of the El Dabaa area. Additionally, the study found that the lineaments inferred from the 2D resistivity sections (Fig. 10) correspond with the geological map of the study area (Abu Risha and Sturchio 2018).

Conclusion

2D resistivity models have provided a highly detailed, comprehensive, and informative depiction of subsurface resistivity. Notably, they closely matched the geological structure and lithology, thereby demonstrating their accuracy. These models have been successful in highlighting a number of contrasts and discontinuities in the subsurface. These include the identification of subsurface structural features, an abrupt lateral change in facies, and the spatial distribution of conductive zones. The most obvious finding to emerge from this study is that the fence diagrams of both 2D resistivity and apparent porosity sections show possible connections between the aquifers of oolitic limestone of the Pleistocene age and fractured limestone of the Middle Miocene age. In addition, there is a channel-like structure near VES stations D23, D13, and D25 (~ 150 m deep from the surface). The second major finding was the identification of a low resistivity zone in the northern region of the research area. This was discovered through the use of a 2D inversion scheme, which indicates the presence of saline water (SW) in the area. There is evidence to support this conclusion.

In conclusion, 2D resistivity inversion is a powerful technique for determining subsurface resistivity distributions using electrical sounding. Prior information and other constraints can enhance the accuracy and reliability of the inversion, resulting in improved geologic interpretations. This development is particularly significant because it can help developing countries that may not have access to expensive multielectrode equipment and reprocess the large volume of legacy 1D resistivity data. It is highly recommended that more studies be conducted on this subject in the future where this research has thrown up many questions in need of further investigation.

Author contributions F Zarif, M Barseem, A Elshenawy and E Ulugergerl: Share in Material preparation, data collection and analysis. The first draft of the manuscript was written by [FZarif] and all authors commented on previous versions of the manuscript. All authors read and approved the final manuscript.

Funding Open access funding provided by The Science, Technology &Innovation Funding Authority (STDF) in cooperation with The Egyptian Knowledge Bank (EKB). Authors confirm No external funding from funding agencies in the public, commercial, or not-for-profit sectors.
Open access funding provided by The Science, Technology & Innovation Funding Authority (STDF) in cooperation with The Egyptian Knowledge Bank (EKB).

Data availability No datasets were generated or analysed during the current study.

Declarations

Ethical approval "All authors have read, understood, and have complied as applicable with the statement on "Ethical responsibilities of Authors".

Competing interests The authors declare no competing interests.

References

Abdallah AM (1966) Stratigraphy and structure of a portion in the northwestern desert of Egypt U.A.R. (El Alamein– Dabaa-Qattara-Moghra area) with reference to its economic potentialities. Geol Surv Egypt Paper no 45:1–19
Abdel Latif TA Geophysical studies on underground water in some localities between Ras El Dabaa and Ras El Hekma, northwestern coastal zone, Egypt., Thesis PD (1973) Fac. Sci., Cairo Univ., Cairo
Abu Risha UAA, Sturchio N (2018) The impact of hydrogeological setting on the protection of coastal groundwater aquifers, El Dabaa, Northwestern Coast, Egypt. J Basic Environ Sci 5:174–186
Adams KH, Hamlington B, David C, Reager J, Sawyer A, Buzzanga B, Fredericks J (2023) Estimating saltwater intrusion using remote-sensing datasets and analytical approaches, EGU General Assembly, Vienna, Austria, 24–28 Apr 2023, EGU23-3641, https://doi.org/10.5194/egusphere-egu23-3641, 2023
Agoubi B (2021) A review: saltwater intrusion in North Africa's coastal areas—current state and future challenges. Environ Sci Pollut Res 28:17029–17043. https://doi.org/10.1007/s11356-021-12741-z
Archie GE (1942) The electrical resistivity log as an aid in determining some reservoir characteristics. Trans AIME 146:54–67
Atwia MG, Abu-Heleika MM, El-Horiny MM (2013) Hydrogeochemical and vertical electrical soundings for groundwater investigations, Burg El-Arab area, Northwestern Coast of Egypt. J Afr Earth Sc. https://doi.org/10.1016/J.JAFREARSCI.2012.11.001
César AM, Lívia PIH, Ariane, Raissa PC (2017) Dc resistivity method applied in the monitoring of diesel leakage in a railway accident in são manuel city, são paulo state (Brazil). https://doi.org/10.22564/RBGF.V35I1.969
Alzahrani H, Abdelrahman K, and Hazaea SA (2022) Use of geoelectrical resistivity method for detecting near-surface groundwater potential zones at Riyadh city, Saudi Arabia, *Journal of King Saud University*. 34:102253.
Constable SC, Parker RL, Constable CG (1987) Occam's inversion: a practical algorithm for generating smooth models from electromagnetic sounding data. Geophysics 52(3):289–300
Cook PG (2003) A guide to regional groundwater flow in fractured rock aquifers. CSIRO Land and Water, Glen

Desert Research Center (DRC) (2005) Geophysical investigation study for groundwater resources in the area of agricultural development project in Sedi Abdel Rahman area-El Hamam canal extension. Internal Report

Desert Research Center (DRC) (2008) Geoelectrical Resistivity Survey for the Sonak Al Ahlyah for Commerce Co. Al Alamein Airport-Northwestern Coast. Internal Report

Eissa MA, Mahmoud HH, Shouakar-Stash O, El-Shiekh A, Parker BL (2016) Geophysical and geochemical studies to delineate seawater intrusion in Bagoush area, northwestern coast, Egypt. J Afr Earth Sc. https://doi.org/10.1016/J.JAFREARSCI.2016.05.031

Eissa MA, Shawky HA, Samy A, Khalil MMH, El Malky M (2018) Geochemical and Isotopic Evidence of Groundwater Salinization Processes in El Dabaa Area, Northwestern Coast, Egypt. https://doi.org/10.3390/GEOSCIENCES8110392

Ekinci YL, Demirci A (2008) A damped least squares inversion program for the interpretation of Schlumberger sounding curves. J Appl Sci 8(22):4070–4078

El Maghraby M (1997) Geophysical, hydrogeological and remote sensing studies on the effect of sea level fluctuation on the groundwater reservoir between Alexandria and El Dabaa, Egypt. Ph.D. Thesis, Alex. Uni. 357p

El-Qady G, Sakamoto C, Ushijima K (1999) 2D inversion of VES data in Saqqara archeological area. Egypt Earth Planet Space 51:1091–1098

Elasy EM, Turnadge C, Werner AD (2018) A three-dimensional variable-density flow model to assess saltwater intrusion in a coastal aquifer. AGU Fall Meeting Abstracts

Eleraki M, Gadallah M, Gemail K, Attwa M (2010) Application of resistivity method in environmental study of the appearance of soil water in the central part of Tenth of Ramadan City. Egypt Q J Eng Geol Hydrogeol - Q J ENG GEOL HYDROGEOL 43:171–184. https://doi.org/10.1144/1470-9236/08-079

Embaby A, Ahmed A, Mahran T, Elsayed A, Masoud A (2023) Effects of Groundwater Abstraction and Desalination Brine Injection on a Middle Miocene Aquifer of the El-Dabaa Area, Northern Coast of Egypt. Sohag J Sci 8(1):41–46. https://doi.org/10.21608/sjsci.2022.171452.1042

Ertekin C, Ulugergerli EU (2022) Geoelectrical survey over perched aquifers in the northern part of Upper Sakarya River Basin, Türkiye. Journal of Groundwater Science and Engineering, 2022, 10(4): 335–352. https://doi.org/10.19637/j.cnki.2305-7068.2022.04.003

Eze SU, Orji OM, Abriku EO, Saleh SA, Abolarin MO (2022) Integrated Geoelectrical Resistivity Method for Environmental Assessment of Landfill Leachate Pollution and Aquifer Vulnerability studies. J Geoscience Environ Prot. https://doi.org/10.4236/gep.2022.109001

Fajana AO (2020) Groundwater aquifer potential using electrical resistivity method and porosity calculation: a case study. NRIAG J Astron Geophys 9(1):168–175. https://doi.org/10.1080/20909977.2020.1728955

Flathe H (1955) Possibilities and limitations in applying geoelectrical methods to hydrogeological problems in the coastal areas of North West Germany. Geophys Prospect 3(2):95–109

Fouad F, Sh (2001) Vertical electrical soundings investigation in northwestern Egypt; a case study in a coastal area. J. of African Earth Sci., Vol. 33, Issues 3–4, pp. 673–686

Frischknech FC, Smith BD, Hoover DB, Long CL (1933) New applications of geoelectrical methods in Mineral Resource Assessment. US Geological Survey Circular, p 221. 980–986

G¨unther T (2004) Inversion methods and resolution analysis for the 2D/3D reconstruction of resistivity structures from DC measurements Dr Rer Nat Thesis Fac. Geowissenschaften, Geotechnik und Bergbau der Technischen Univ. Bergakademie Freiberg, Germany, Geophys. 65 97–110

Glover PW, Hole MJ, Pous J (2000) A modified Archie's law for two conducting phases. Earth Planet Sci Lett 180(3–4):369–383

Goto TN, Kasaya T, Machiyama H, Takagi R, Matsumoto R, Okuda Y, Kinoshita M (2008) A marine deep-towed DC resistivity survey in a methane hydrate area, Japan Sea. Explor Geophys 39(1):52–59

Henry-Poulter, S.A., M.Z. Abdullah, A.M. Binley and F.J. Dickin (1993) Electrical impedance tomography of tracer migration in soils, In: Computational methods and Experimental Measurements IV, Vol 1: Heat and Fluid Flow, by Brebbia and Carlomagno, eds., Computational Mechanics Publications, pp. 101–115.

Hossam M, El A, Zaher M, Shokry AS, Mahmoud IIM (2021) Geophysical investigation for sustainable development at Alamein Area, Northwestern Coast, Egypt. Egypt J Aquat Res. https://doi.org/10.1016/J.EJAR.2020.07.002

Hossam M, El, Khafagy M, AbouShagar AL, Abdel Fattah TH (2023) Groundwater Investigation Using Electrical Resistivity Method at New Borg El-Arab City, Alexandria, Egypt. Egypt J Aquat Res. https://doi.org/10.1016/j.ejar.2022.12.001

Housny HM (2011) Contribution of geoelectrical survey methods in studying the condition of groundwater occurrence in El Alamin Area-Northwestern Coast-Egypt. EGS J 9(1):181–189

interpex (2023) http://www.interpex.com/ftp/ix1d/ix1dv3setup.exe AD 01/12/2023.

Kaidi X, Man L, Zhiyong Z, Ke Y, Feng Z (2023) Two-dimensional Inversion of DC Resistivity Data on Unstructured Grids Using Fuzzy C-means Clustering Model Constraint. Journal of Environmental and Engineering Geophysics 2023; 27 (3): 135–147. https://doi.org/10.32389/JEEG22-028

Khalil MA, Santos FAM (2011) 2D resistivity inversion of 1D electrical-sounding measurements in deltaic complex geology: application to the delta Wadi El-Arish, Northern Sinai, Egypt. J Geophys Eng 8(3). https://doi.org/10.1088/1742-2132/8/3/003

Kotb ADM, Khaled MA, Barseem MS (2018) Groundwater condition based on geoelectrical technique and Dar Zarrouk parameters between El Alamein and El Dabaa—Egypt. Arab J Geosci 11(19). https://doi.org/10.1007/s12517-018-3947-y

Loke MH, Barker RD (1996) Rapid least-squares inversion of apparent resistivity pseudosections by a quasi-newton method Geophys. Prospect 44:131–152

Luz EDC, Régis CRT (2009) Influence of sea water resistivity on MCSEM data. Revista Brasileira De Geofísica 27:349–356

Magesh NS, eshlal KV, Chandrasekar N, Anand (2012) Electrical resistivity mapping and 2D resistivity imaging for saltwater intrusion studies in coastal aquifers. Environ Earth Sci 67(6):1715–1721

Marescot L, Palma Lopes S, Rigobert S, Lagabrielle R, Chapellier D (2005) Non-linear resistivity inversion on 3D structures with complex shaped 11th European Meeting of Environmental and Engineering Geophysics: Proc. of the Near Surface (Palermo, Sept 2005)

Marina A, Martin S, Andreas G, Robert S, Jürgen W (2021) Reconstruction of former channel systems in the northwestern Nile Delta (Egypt) based on corings and electrical resistivity tomography (ERT). EG Quaternary Sci J. https://doi.org/10.5194/EGQSJ-70-151-2021

Massoud U, Soliman M, Taha A, Khozym A, Salah H (2015) 1D and 3D inversion of VES data to outline a fresh water zone floating over saline water body at the northwestern coast of Egypt. NRIAG J Astron Geophys. https://doi.org/10.1016/J.NRJAG.2015.11.001

Meju MA (1994) Geophysical Data Analysis: understanding Inverse Problem Theory and Practice: SEG Course Notes Series, vol 6. Tulsa:SEG

Menke W (1989) Geophysical data analysis: discrete inverse theory. Acad Press. https://doi.org/10.1016/C2011-0-69765-0

Merrick NP (1997) A new resolution index for resistivity electrode arrays. Exploration Geophysics 28:106–109.

Monteiro Santos FA, Sultan SA (2008) On the 3D inversion of vertical electrical soundings: application to the South Ismailia area—Cairo Desert Road, Cairo. Egypt J. Appl.Osmond, South Australia

Özürlan G, Candansayar ME, Şahin HM (2006) Deep resistivity structure of Dikili- Bergama region, West Anatolia, revealed by two dimensional inversion of vertical electrical sounding data. Geophys Prospect 54:187–197. https://doi.org/10.1111/j.1365-2478.2006.00525.x

Rijo L, Pelton WH, Feitosa EC, Ward SH (1977) Interpretation of apparent resistivity data from Apodi Valley, Rio Grande DoNorte, Brazil. Geophysics 42:811–822. https://doi.org/10.1190/1.1440749

Sampson ES, Ibitoye T, Saleh SA, Nworu JS (2018) Studies of Salt Water intrusion in Opobo/Nkoro Rivers State Using Geophysical and Hydrochemical Methods. Journal of environment and earth science, Journal of Environment and Earth Science www.iiste.org, ISSN 2224–3216 (Paper) ISSN 2225 – 0948 (Online) Vol.8, No.11, 2018

Saqr A, Abd-Elmaboud M (2024) Saltwater intrusion in Coastal aquifers: a Comprehensive Review and Case studies from Egypt. https://doi.org/10.32388/XLIS2F

Sayed MA (1967) Geophysical study on the groundwater resources of Ras El-Hekma area, northwestern littoral zone of Egypt, M.Sc. Thesis, Fac. of Sci., Cairo Univ., 129 pp

Shata A (1955) An introductory note on the geology of the northern portion of the western desert of Egypt. Bull Inst Desert 5(2):96–106

Shata A (1971) The geomorphology, pedology and hydrogeology of the Mediterranean coastal desert of the A. R. E. Symposium of the Geology of Libya. pp. 431–446

Uchida T (1991) Two-dimensional resistivity inversion for Schlumberger sounding Geophys. Explor Japan (Butsuri Tansa) 44:1–1

Ulugergerli EU (2017) Marine effects on vertical electrical soundings along shorelines. Turkish J Earth Sci 26(1):57–72. https://doi.org/10.3906/yer-1610-10

Vedanti N, Srivastava RP, Sagode J et al (2005) An efficient 1D Occam's inversion algorithm using analytically computed first- and second order derivatives for DC resistivity soundings. Comput Geosci 31(3):319–328

Yousif M, Bubenzer O (2015) Geoinformatics application for assessing the potential of rainwater harvesting in arid regions. Case study: El Daba'a area, Northwestern Coast of Egypt. Arab J Geosci 8(2015):9169–9191

Zaghloul M (2020) Exploring groundwater aquifers using geoelectrical techniques in wadi sakhr and its vicinities, northwestern coast, Egypt. https://doi.org/10.21608/EJDR.2021.50869.1077

Zarif F, Slater L, Mabrouk M, Youssef A, Al-Temamy A, Mousa S, Farag K, Robinson J (2018) Groundwater resources evaluation in calcareous limestone using geoelectrical and VLF-EM surveys (El Salloum Basin, Egypt). Hydrogeol J 26:1169–1185. https://doi.org/10.1007/s10040-017-1710-1

Zarif FM, Elshenawy AM, Mabrouk MA (2021) Integrated TEM and 2DERI techniques to delineate groundwater bearing zones in fractured carbonate rocks at the upstream portion of Wadi Halazeen, Northwestern Coast, Egypt. J Afr Earth Sc 182. https://doi.org/10.1016/j.jafrearsci.2021.104288

Zarif FM, Elshenawy AM, Barseem MS, Al-Abaseiry AA, ElSayed AN (2022) Evidence of geoelectrical resistivity values on groundwater conditions in Wadi El Natrun and its vicinities, West Delta, Egypt (cases studies). Dent Sci Rep. https://doi.org/10.1038/s41598-022-12644-0